High-Voltage Solar Cell Modules in Simulated Low-Earth-Orbit Plasma

Heinz Thiemann*
Physikalisch Technische Studien GmbH, Freiburg, Federal Republic of Germany

and

Klaus-Peter Bogus†
ESA Technical Directorate, Noordwijk, The Netherlands

Solar cell modules operated at high voltages in a surrounding simulated low-Earth-orbit plasma have been investigated over an applied voltage range from −700 up to +500 V. The main objective was to characterize the behavior of current European technology solar cell modules and to improve the understanding of the underlying interaction processes. The measurements were performed in a large (2.5-m diameter by 5-m length) chamber under high vacuum using Argon ions from a Kaufman source to generate a high-density plasma up to 10^6 cm^{-3}. Measurements of the overall current collection characteristics were performed in combination with near-range measurements of potential and particle density distribution in the vicinity of coverglasses and cell interconnectors. The results support the hypothesis that secondary electrons contribute to the anomalous current increase observed at positive module voltages above 300 V. The surface potential on the coverglasses of the solar cells increased only in the vicinity of the interconnectors to high values, and the previously reported "snap-over" of the high interconnector potential across the entire coverglass surface at high positive voltages could not be reproduced. Moreover, it was found that the prehistory of the test samples influences the quantitative results of the measurements.

I. Introduction

A SIGNIFICANT increase of the solar array operating voltage from the conventional levels of 28–42 in the U.S. and 50 V in Europe is required in order to provide future large platforms and space stations in Low Earth Orbit (LEO) with 10–100 kW electrical power without excessive mass and/or plasma power losses of the solar generator harness. Currently, bus voltages between 100 and 200 V are under consideration. Taking into account the ratio between bus voltage and maximum solar array open circuit voltage (about 1 : 2) and the ratio between operational voltage and development/qualification test levels, it becomes obvious that the voltage range to be investigated is 200–600 V.

The interaction between elevated-voltage solar arrays and the surrounding high-density plasma in LEO has been studied in the past in numerous ground simulation tests and in a few flight experiments. Ground tests cannot definitely reveal the interaction features of solar arrays with the LEO-plasma environment due to the difficulties in 1) simulating a realistic LEO plasma and 2) testing a solar array of actual dimensions. Nevertheless, they are a first step in obtaining information about current collection processes of a solar array operating at elevated voltages in a plasma environment.

The tests reported here were aimed at improving the understanding of the basic processes that control the interaction of elevated-voltage solar arrays with the surrounding LEO plasma. This is accomplished by combining measurements of the overall current collection characteristics of representative solar cell test modules with measurements of near-range effects in the vicinity of the solar cell interconnectors and coverglass edges. An evaluation of previous studies and tests performed mainly in the U.S. and, at a preliminary level, in Europe, is summarized in Sec. II. Section III contains a description of the plasma simulation facility and the test samples used. The tests and experiments and their corresponding results are described in Sec. IV. Section V contains a discussion of the major findings and an interpretation of the results in a preliminary model.

Received July 17, 1986; revision received Jan. 21, 1988.

*Senior Research Scientist.

†Head of Solar Generator Section.

II. Review of Previous Investigations

The complexity of the interactions between solar arrays and the plasma environment is reflected in a multitude of publications reporting on general and specific aspects in this area. Purvis et al.[1] found that current collection of a positively biased module with 2 × 4 cm solar cells is confined to the interconnect region if the applied voltage is less than +190 V. At larger voltages, a transition in the collection phenomenon was observed, associated with a sudden change in the surface voltage profile of the segment. At this "snap-over," the bias voltage expands from the interconnectors to encompass the cover slides as well. The authors concluded that snap-over conditions occur due to secondary electron emission from the cover slides. The module arcs if it is biased negatively to a value beyond −700 V.

These tests were performed at a plasma density of 1E5 ions/electrons per cm^3 using N_2 as working gas. At lower ambient plasma densities, the voltage onset for arcing was shifted toward higher values.

Stevens et al.[2] found that insulator surfaces surrounding biased conductors strongly influence the interactions with the plasma environment. Using solar cells of 2 × 2 cm surface area and positive voltages greater than the snap-over voltage of +100 V, the ground simulation testing data indicate that the dielectrics add to the current collection area.[3] For negative voltages beyond −500 V, the dielectrics contribute to the observed discharges. Strong electric fields near the cell interconnectors were assumed to trigger discharges.[4]

The snap-over effect was explained by Stevens[4] with a simple sheath model. This model was based on a phenomenological model using hemispherical sheaths forming around the interconnects, which expand radially as the applied voltage increases. Above a certain voltage, the sheaths of adjacent interconnects overlap, and finally a nearly planar sheath structure develops in front of the module surface.

A sheath radius of about 1 cm was calculated at about +100 V, resulting in sheath overlap for 2 × 2 cm cells. Additional tests conducted on a 20-cell module of 2 × 4 cm cells showed a snap-over between 160 and 190 V.[4]

The influence of ambient magnetic fields was studied by Grier.[5] Generally, the magnetic field increased the plasma coupling current for negative biases. A more complex behavior was found in the positive voltage range, where an increase or decrease in the current was observed in the presence of magnetic fields, depending on other parameter settings like the voltage, electric field strength, and plasma density. Anyway, the currents collected with and without magnetic field were not sufficiently different to require a fundamentally different interaction process in the presence of a magnetic field. Therefore, magnetic field effects were not further investigated here.

Other aspects of the interaction process were investigated experimentally by McCoy et al.[6] With a model array using an electronically conducting front surface with a dielectric border along all edges, they measured plasma sheath dimensions formed about this high-voltage panel and the sheath current leakage. These measurements were mainly intended to determine the feasibility of this type of simulation and the order of magnitude of the quantities involved.

The temporal aspects of current collection were investigated by Stillwell et al.[7] Electron currents collected through small insulation defects showed occasional transients of large magnitude associated with material degradation due to energetic bombardment of electrons. This effect was not reported in earlier studies.

A possible way to prevent arcing was recently proposed by Ijichi et al.[8] Based on an analysis of space plasma interactions, these authors suggested conductive coating of the solar-cell coverglasses, similar to that used on the ESA satellites Geos and ISEE-B for other reasons.

Theoretical considerations include estimates of power losses based on calculations of space-charge-limited sheath dimensions.[6] It was concluded that the current collected should not be a function of the detailed surface structure of the collecting array. This result, which is in contrast to our findings, implies sheath structures that average out the effects of small-scale voltage and current variations at the collector surface.

A modified version of the NASCAP (NASA Satellite Charging Analyzer Program) model computes LEO current collection effects by using a simplified screening model for the electrostatic potential, with user-specified potential contours.[9] The importance of dynamical calculations[10] and the influence of new particle populations[11] were realized by performing self-consistent two-and-a-half-dimensional particle simulations, with possible secondary electron emission from a dielectric. Though these authors start with the unrealistic assumption of equal ion and electron mass, the calculated potentials on the dielectric surface already show the complicated features of the interaction process, which finally determines the current-collection properties of solar array structures in the LEO environment.

III. Test Facility and Test Samples

The plasma facility is a large cylindrical vacuum tank that simulates the terrestrial ionosphere. The cylindrical dimensions provide a working space of 2.5 m in diameter and 5 m in length (Fig. 1). The pressure inside the chamber was maintained near 10^{-6} Torr and monitored by a pressure gauge within the chamber. Operating the chamber with plasma yields a pressure of 10^{-5} Torr. The plasma is generated by a source of the Kaufman type, where Argon ions are extracted via the dc discharge from the ionization volume and neutralized by the negative space charge emitted by the heated neutralizer filament. This results in a directed plasma beam with energies between 10 and 100 eV.

The accomplished values of the simulated LEO-plasma were $N_e = 10^5$ up to 10^6 cm^{-3} and $T_e = 0.1$–0.3 eV. The test sample, which was electrically isolated from the tank ground, generates a local distortion of the plasma density distribution. Density gradients of 20% within a distance of 50 cm perpendicular to the module were observed. In the parallel direction, a fairly constant density profile exists. Behind the module, a wake-like structure forms. Though density gradients are an artifact of this source, it is believed that this configuration reproduces orbit conditions adequately.

For the tests, standard plasma conditions were defined as $N_e = 8 \times 10^5$ cm^{-3}, $T_e = 0.1$ eV, and compensated Earth magnetic field. The plasma tests were performed with test modules representing small fractions of a high-voltage solar cell string consisting of 20 solar cells (2 × 4 cm) in series connection. The intercell gap was 0.9 mm. The module was mounted on a Kapton substrate with a total area of about 600 cm^2.

A bias voltage was applied to the solar cell module, simulating the local solar cell voltage of a high-voltage array as it is governed by the position of the module on the string and by the overall bus voltage. Variation of the bias voltage in the positive range from 0 up to about 2% of the maximum array voltage and in the negative range from 0–98%, therefore, simulates a complete scan across the entire array string in LEO equilibrium conditions, assuming a floating solar array configuration.

These voltage ranges result from the zero net current requirement considering positive and negative carriers collected by the array in equilibrium. Leakage currents flowing through the plasma between the biased module and the chamber walls were measured by an electrometer in the current loop. The various interconnects between the solar cells of the module are almost at the same potential because the plasma currents flowing through the solar cells are too small to produce a substantial potential drop across the cell.

The absolute electron density was measured by a standard impedance probe technique.[25] Electron temperature measurements were performed with a planar retarding potential ana-

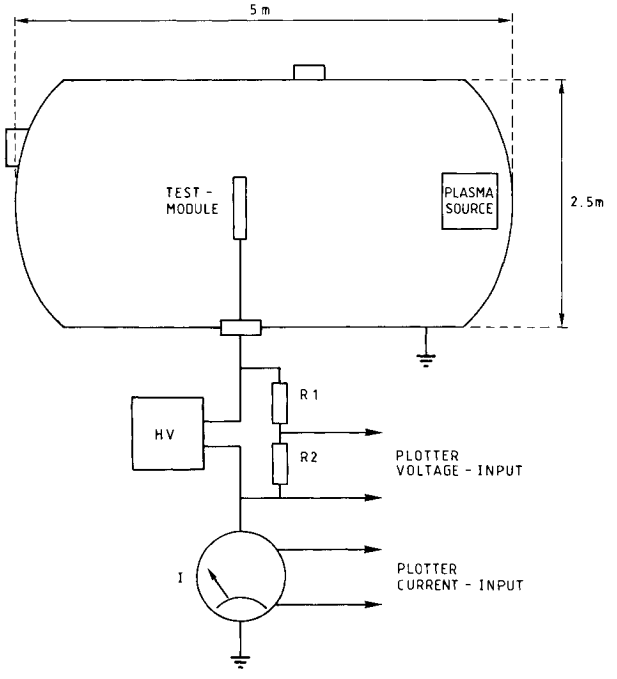

Fig. 1 Experimental setup.

lyzer.[26] Relative electron and ion density measurements were made using a thin cylindrical Langmuir probe calibrated with the impedance probe. The Langmuir probe was operated in the electron or ion saturation mode, typically +5 V beyond the automatically determined floating potential of the probe. Potential measurements in the plasma were made with a small half-spherical sensor connected to a high-input impedance (10^{16}-ohm) electrometer of the electric field mill type. The same technique was applied for surface potential measurements, with the probe contacting the surface. The profiles were measured in a discrete mode, where the probe was first discharged. The equilibrium potential value was usually obtained within one second. In view of the large internal time constant of the instrument ($t = 10^5$ s), the measured values are considered as true local plasma potentials.

IV. Results

The basic features of current collection by a solar array test module are summarized in Fig. 2. This example shows all characteristic features as they can be observed in the negative and in the positive bias voltage domain on a single module.

A. Negative Bias Voltage Effects

Figure 2b shows the ion collection mode for negative applied voltage up to −700 V. While no anomalous current collection is observed, arcing effects set in quite irregularly beyond a voltage threshold of −500 V.

In addition to the current voltage characteristic (CVC), measurements of the plasma potential distribution in front of the module were made as a function of distance from the surface for negative bias voltages below the arcing threshold. Figure 3 shows the perpendicular profile for three different applied module voltages ($Z = 0$ is the test sample position). We note a decrease of the barrier height as the applied voltage becomes more negative.

The impact of ions may in principle cause secondary electron emission from the module surface. Since no anomalous current increase is seen in the corresponding CVC (Fig. 2b), there can be no significant contribution of additional charged particles to the leakage current in the ion collection mode.

The discharges beyond −500 V are comparable with those in the positive voltage range described hereafter. However, additional glow discharge effects are observed along the solar cell edges in the surrounding plasma, which produce the smaller current spikes on the CVC. The system almost immediately recovers after the arcing process. Arc discharges modify the physical properties of the module and can change the geometry around the interconnects by degradation of solar cell or interconnect material. An example is given in Fig. 4, which shows the degradation of interconnect and solar cell material. Arcing effects occurring in the positive and negative voltage ranges are generated by different processes. Using the same test module for studies in the positive and negative voltage ranges leads to a mixture of typical features in the different voltage regimes. This modifies the interaction process in the individual voltage

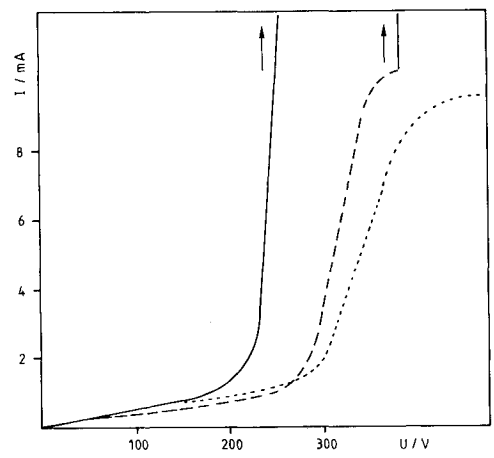

Fig. 2a Current voltage characteristics of the solar array test module (electron mode).

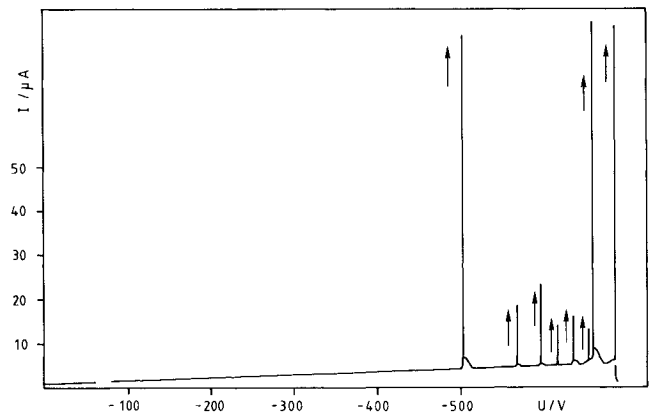

Fig. 2b Current voltage characteristics of the solar array test module (ion mode).

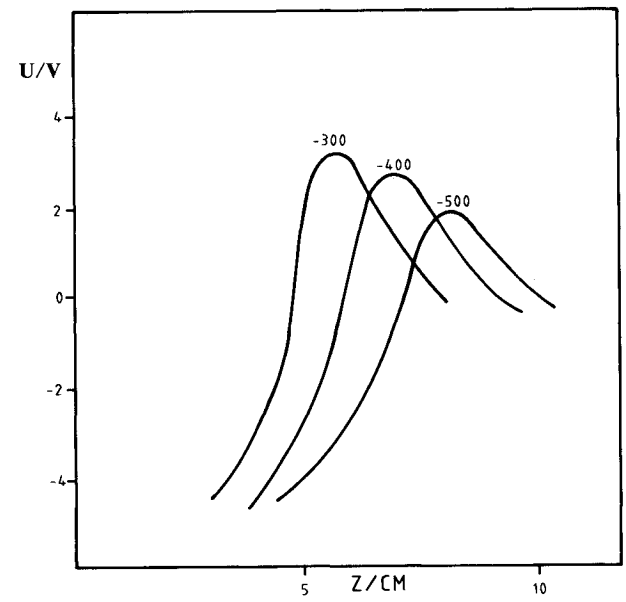

Fig. 3 Formation of potential barriers in the ion mode.

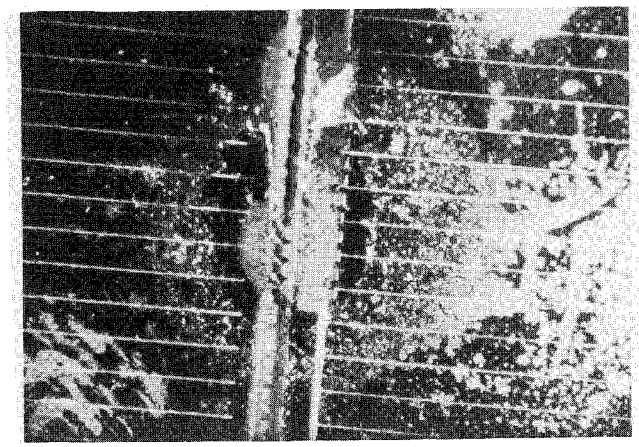

Fig. 4 Degradation of interconnector and solar cell material due to arc discharges.

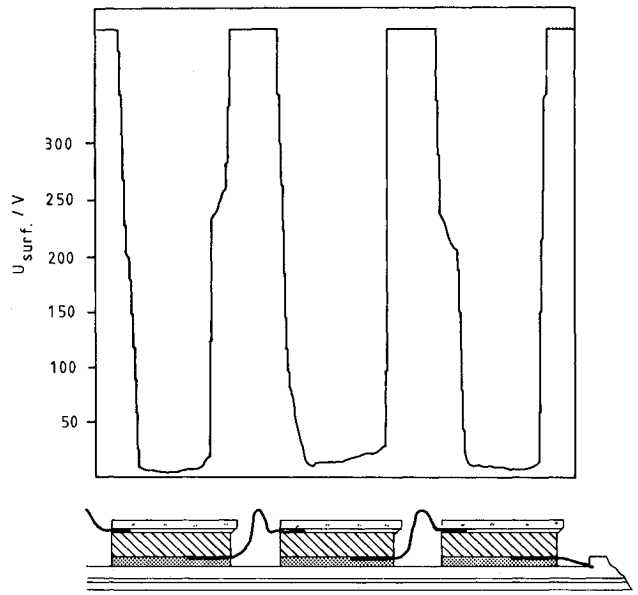

Fig. 5 Surface potential profiles across three solar cells of the module biased at ±400 V.

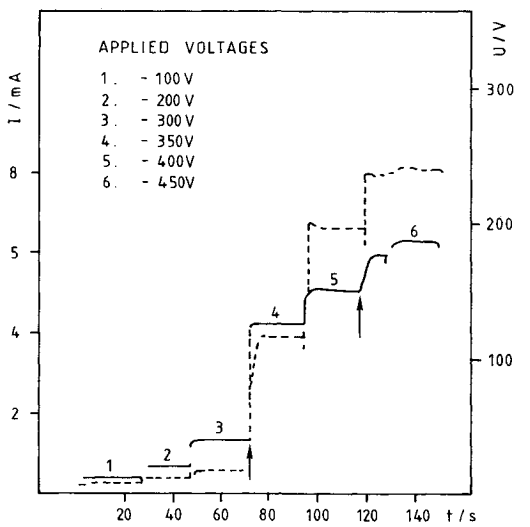

Fig. 6 Correlation between anomalous current (dashed line), increase of the test module, and surface potential (full line) enhancement at the coverglass edge.

ranges in an unrealistic way. Therefore, we basically confined the measurements to the more complex positive voltage range, and measurements in the negative voltage range were limited to the identification of arcing effects.

B. Positive Bias Voltage Effects

Figure 2b shows current-voltage characteristics (CVC) for positive voltages up to 500 V. The three curves characterize the properties of the test module in its virgin state (full line), after two months of daily testing (dashed line), and in its final state after three months. Each day, 30 test runs of 5 min duration each were performed, resulting in a recording of the complete CVC.

We distinguish between two different voltage regimes characterized by (1) normal and (2) anomalous (increased) current collection, respectively. The transition occurs at a critical voltage U_c. The critical voltage is not a well-defined value but is influenced by the configuration of the module, its history, and its mode of operation. The CVC is not a reproducible curve over the displayed voltage range. In the beginning, the anomalous current terminates in arcing, which is marked by arrows in Fig. 2. These arc discharges change the CVC fundamentally by shifting the critical voltage onset for anomalous current collection to higher values and also extending the normal current mode. The curves are only reproducible and stable over voltage ranges below the arc discharge threshold. Arcing appears to be a phenomenon related to explosively increasing current collection and visually observed local discharges on the module predominantly between selected interconnects and the dielectric parts of the solar cells. The arcing centers suddenly (sometimes gradually) disappear during operation. New arcing centers appear at higher voltages in other locations of the module. Finally, all previous arcing centers appear to be modified in such a way that arc discharges are only observed at bias voltages above +500 V. Now a reproducible behavior is obtained for the same ambient plasma conditions (dotted line). An increased current with a saturation level of about 10 mA is observed, exceeding the normal current by one order of magnitude.

Systematic studies are possible in the domain where no arcing phenomena occur (as characterized by the dotted curve of Fig. 2b). In this configuration, the response of the environment was studied in more detail in order to derive the fundamental properties of plasma-module interactions. This included the measurements of the lateral potential distribution across the solar cell module surface and the measurement of the near-range potential distribution in the plasma as a function of the distance from the module surface.

Figure 5 shows some lateral potential distribution details. The surface potential profiles for three adjacent solar cells are recorded after the onset of anomalous current collection for an applied voltage of +400 V. The exact module voltage is measured on the six metallic interconnectors. On the dielectric coverglass surface, we note a characteristic potential structure with elevated surface potentials in the vicinity of the interconnectors decreasing steeply and forming a broad potential valley in the center region. There is no precise reproducibility in the measured profiles, and the potentials differ in their magnitude, shape, and extension into the dielectric surface. A further increase of the applied voltage does not cause a significant widening of elevated potential structures near the interconnectors. Such potential profiles are in contrast to uniformly increasing potentials across the whole solar cell surface, reported earlier[4] at a certain snap-over voltage.

A clear correlation between the onset of anomalous current collection and the formation of significant surface potentials at the coverglass edges is demonstrated in Fig. 6. Here, the test module is operated in a "discrete" mode, i.e., a stepwise increase of the bias voltage. We see the temporal evolution of the current for the indicated applied voltages (full line) and of the corresponding surface potentials measured on the dielectric solar cell coverglass cell near the interconnector (dashed line). The arrows indicate the instant of voltage increase. We note a direct correlation between the magnitude of the current step and the magnitude of the surface potential increase near the interconnects. Similar measurements near the central part of the solar cell surface show that the potential in the central area does not increase significantly.

Figure 7 shows the potential distribution in the ambient plasma in front of the module in relation to the current collection modes. The current drawn by the test module is again measured in the discrete mode. The potential profile perpendicular to the module surface is simultaneously measured for defined positive bias voltage steps, starting near a metallic interconnector. The interconnector potential of 250 to 400 V drops down to plasma potential levels below 10 V on a very short distance below the resolution at the chosen Z scale. By moving the probe in the axial Z direction, the current collection properties of the module are slightly influenced, as can be seen from the dip in the temporal current curve. The relative current decrease due to this measurement, however, is small

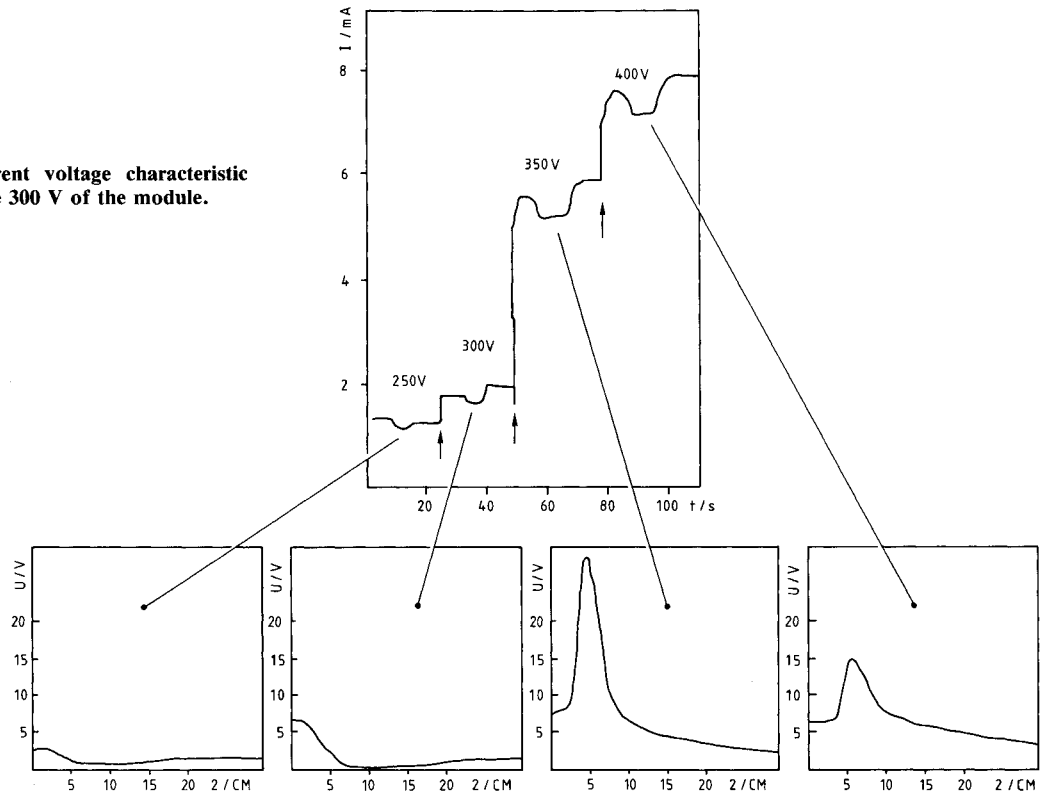

Fig. 7a Current voltage characteristic showing above 300 V of the module.

Fig. 7b Potential profile in front of the module at various bias voltages.

compared to the equilibrium current level and therefore negligible. In the normal current mode ($U = 300$ V), the perpendicular potential profiles show smooth behavior with a potential hump near the module, which increases with the applied voltage.

The transition to anomalous current collection occurs at $I = +350$ V and shows a fundamental change in the external potential structure. In the state of increased current collection, a potential barrier of 25 V is forming about 5 cm in front of the test module. Such potential structures are not typical for sheath formations around single probes but show more similarity with double-layer-type structures. Further increased module voltage leads to a reduction of the potential barrier. For $U = +500$ V, the occurrence of arcing disturbed the measurement.

The electric fields originating from the biased interconnectors are strongly shielded by the plasma. The probe dimensions (0.2-cm diam) are too large to resolve any potential structure between the interconnector and the plasma, characterizing the transition from large applied to small plasma potential values. Even for very large applied voltages, we cannot detect any expansion of the plasma sheath near the interconnector, as would be expected according to a simple probe theory.

Anomalous current collection requires additional charge carriers, which can be generated by one of the following mechanisms: 1) secondary electron emission from the insulating solar cell material,[11] 2) vaporization of the insulator material and subsequent ionization,[12] and 3) ionization of the neutral background gas.[13] The generation of additional ions near the surface and beyond the critical voltage was verified by ion density measurements. The ion density in arbitrary units is shown in Fig. 8 by the solid line as a function of the bias voltage. The dotted line represents the plasma potential measured simultaneously by a second probe. Both probes were separated about 2 cm from each other and located 2 cm in front of the module. The plasma potential remains nearly unaffected up to the critical voltage, while the ion density shows a shallow minimum at about 200 V. Near the critical voltage $U_c = 300$ V, we note first

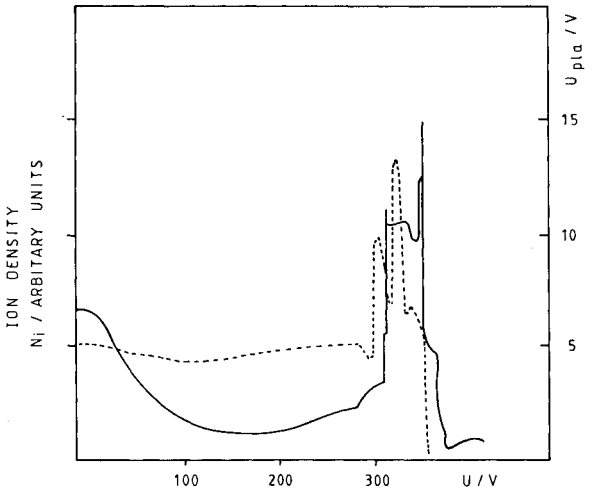

Fig. 8 Secondary plasma generation due to the formation of a potential barrier. Dotted line = barrier potential; full line = relative ion density.

a sudden increase in plasma potential, then with a voltage offset of 10 V, a sudden ion density increase. The increased potential persists over a voltage range of 30 V, and a similar coverage is observed in the increased ion density.

This behavior is consistent with Fig. 7, where a potential barrier is identified in front of the module. At a distance of 2 cm in front of the module, the probe is not at the location of the potential maximum, hence the relatively lower potential value. The retarded onset of an increased ion density after the potential rise can be interpreted such that a certain potential structure has to develop in order to allow the formation of additional ions. These ions are not the result of impacting energetic electrons on the different surfaces of the test module

but originate from processes occurring in the environment of the potential barrier. With a relative potential difference of 25 V, the barrier exceeds the ionization potential of the constituents of the neutral background gas (argon, oxygen, or nitrogen). At higher applied voltages, the potential barrier decays (Fig. 7), and the plasma electrons can no longer be energized. Consequently, the ion density decreases drastically.

V. Discussion

The experimental results demonstrate that the interactions of positively biased solar array test modules with a simulated LEO plasma environment are primarily characterized by passive and active processes. While the passive mode is satisfactorily described by normal (Langmuir-probe-type) current collection, LP considerations do not apply to the active mode (anomalous current, arcing), where secondary particle populations are generated, and the global current response of the test module as well as the local response of the plasma environment greatly differ from passive interactions. At the critical voltage, plasma processes between conductive and dielectric parts of the module eventually start interacting.

A. The Plasma/Coverglass Interface

Processes related to the plasma–module interactions, which explain the experimental observations in the different voltage regimes, can be evaluated by referring to a vacuum system. Figure 9a shows the qualitative vacuum potential distribution around a positively biased interconnector. Assuming planar geometry, the applied potential drops linearly toward the grounded plasma chamber walls (representing our potential reference). Polarization of the dielectric coverglass modifies the electric field configuration and results in a discontinuity at the top surface of the coverglass, which is essentially an equipotential line. Smaller fields (compared to the constant-vacuum electric field) are formed inside and larger fields outside the coverglass. The kink in the potential contour lines with associated electric field reversal near the side part of the cell is also related to the polarized material. These potential structures are similar in the positive and the negative voltage ranges for all applied voltage levels. The dielectric surface potentials and potential distribution in ambient plasma differ considerably from this picture. The vacuum electric fields are not maintained in the presence of a simulated LEO plasma, and shielding effects in front of the dielectric and conductive parts, respectively, create new potential structures. Positive polarization charges and surface potentials on the dielectric interact strongly with external electric fields and the ambient plasma. Plasma electrons are accelerated toward the coverglass and compensate the positive polarization charges. At higher bias voltage, even negative surface charges can be produced on the coverglass. Plasma ions, on the other hand, move in the opposite direction and form positive space charges in the distant plasma. This charge separation leaves a diluted plasma near the module. The system reaches steady-state conditions if the net current onto the module surface is zero. This implies lower surface potentials than the undisturbed ambient plasma potential in order to allow for equal ion and electron fluxes. The low surface potentials now define a reversed field configuration with very strong field (of the order of 10^4 V cm^{-1}) inside the coverglass and drastically reduced electric fields outside. The detailed outer field structure is influenced by the ionic space charge, which may be responsible for the potential barrier in Fig. 7, 5–10 cm in front of the cell.

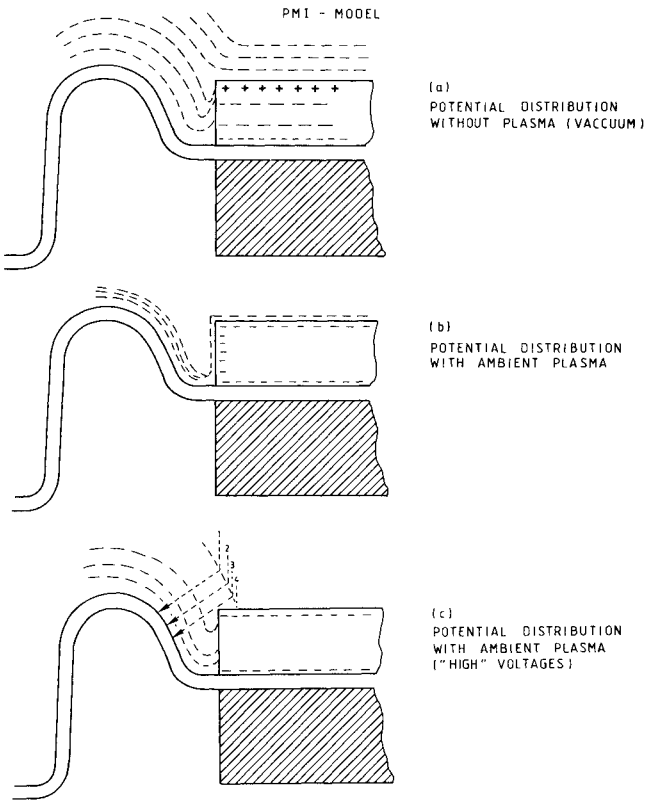

Fig. 9 Qualitative potential distribution for a biased test module in the vicinity of an interconnector.

B. The Plasma/Interconnector Interface

Plasma interactions with the metallic interconnectors *seen in isolation* from their dielectric environment are determined by shielding processes. In equilibrium with zero net current collection, an electrostatic sheath forms around the interconnects, which are acting like plasma probes.[15]

The spatial potential distribution in spherical symmetry for such steady-state potentials is given by

$$\phi(r) = \frac{1}{r} e^{-r/\alpha} \tag{1}$$

where α represents the shielding parameter, which is of the order of the Debye length λ_α. This formula is valid for floating conditions or small probe potentials with $kT_{e,i} \gg e\phi$, where $kT_{e,i}$ represents the thermal energy of electrons or ions, respectively. The particles are assumed to obey Boltzmann statistics.[16]

For highly biased probes, these assumptions are no longer valid. Previous detailed studies[17] dealing with moderate potentials $e\phi = +25kT$, however, confirmed the spatial potential distribution given by Eq. (1). Applying simple Langmuir-Child considerations to a spherical probe,[18] the sheath radius r_{sh} varies with the applied potential according to

$$r_{sh} \sim \phi^{3/7} \tag{2}$$

The electric fields, which are confined within that distance, are considerably larger than the corresponding vacuum fields.

C. The Plasma/Module Interface

Similar potential structures were also found for very large potentials (up to +500 V) in studies on the leakage current collection due to pinhole defects.[19] Although there was qualitative agreement on the spatial potential distribution around the pinhole and its potential dependency, the experimentally measured shielding parameter α was typically one order of magnitude smaller than the expected value: a sheath radius of $r_{sh} = 1.3$ cm only was measured for an applied potential of 458 V and $\lambda_d = 11$ cm (for the corresponding plasma parameters $N_e = 2 \times 10^4$ cm, $T_e = 5.3$ eV). It has been suggested[19] that negative charge accumulation on the insulator surface may lead to this decrease of the electric field penetration into the plasma.

Introducing this scaling 1/10 in our studies with $\lambda_d = 0.3$ cm ($N_e = 5 \times 10^5$ cm^{-3}, $T_e = 0.1$ eV) results in a rough estimate of $r_{sh} = 0.03$ cm for the shielding distance at low potentials, i.e., potentials with plasma sheaths around the interconnector that do not reach the coverglass surface. Figure 9b shows a simplified scheme for the equipotential lines for such a situation in the vicinity of the interconnector. Plasma electrons are able to penetrate into the gap. They create negative surface charges at the edge and at the surface of the coverglass. In equilibrium, the solar cell surface potential is somewhat lower than the undisturbed plasma potential. Large electric fields are forming at the lower coverglass edge, as shown by the concentration of equipotential lines.

Applying Eq. (2), an expansion of the sheath up to 0.1 mm is expected at about 170 V, a value close to the measured critical voltage. At this distance, the sheath edge will reach the solar cell and the steady-state interfaces between plasma and interconnector or coverglass, respectively, are not isolated from each other anymore. The interaction of both interfaces may prevent discharge effects by particles of the undisturbed plasma on parts where the sheath overlaps the coverglass. It also may prevent a free extension of the plasma sheath around the interconnector due to the accumulation of charges on the dielectric. This is supported by the formation of elevated surface potentials on the coverglass edges (Fig. 5).

The schematic equipotential contours for elevated potentials where the sheath reaches the coverglass are sketched in Fig. 8c. Due to the depleted sheath environment and the electric field direction, which deflects charge carriers toward the interconnector, almost no plasma particles are available to reduce the vacuum potentials on the edges of the coverglass. With increasing sheath dimensions, the undisturbed plasma is pushed away from the interconnector environment, and particles impacting on the sheath edge are mostly accelerated toward the interconnector (compare the particle trajectories 1/3 in Fig. 8c). Since the particle flow is deflected, the potential drop along the edge of the coverglass is maintained. This leads to differential charging and local surface potential conditions, which are essential in generating secondary electron emission by energized plasma particles: constant surface potentials across the module surface[15] probably cannot account for increased current collection, since secondary electrons, which obviously have to support this anomalous current, are immediately reflected back onto the surface by the strong electric fields in front of the cell surface. A more plausible explanation is the following: secondary electrons are generated within 50 A of the antireflection MgF-coating (thickness 1500 A).[10] This material shows a broad distribution of a high (above 5) secondary emission yield above 500 eV[21] in contrast to most dielectric materials, which show a yield maximum (~ 3) at a few hundred eV. This explains a further increase of the current at voltages beyond 400 V, which otherwise would decrease when the emission yield decreases.

The yield is significantly increased by the oblique incidence of the plasma electrons (trajectory 4 in Fig. 9c) on the cell corner. For very oblique incidence (e.g., = 80–85 deg), the yield may increase by one to two orders of magnitude.[22] Numerical simulations have shown[11] that the secondary electrons are partially reflected back to the coverglass or emitted into the plasma environment. Secondary electrons flowing into the ambient plasma considerably change the plasma potential distribution. Numerical simulations with a conductive plate emitting electrons into an ambient plasma have shown that a positive potential barrier in front of the plate[13] forms similar to the one shown in Fig. 7.

In order to maintain a stationary charge balance on the coverglass surface in the area of strong secondary electron emission, it is necessary to replenish the electron deficit with electrons from outside this area. Since the bulk conductivity of the dielectric coverglass is far too low, it is assumed that electrons are laterally travelling in the surface potential gradient via charge hopping along the dielectric surface or via surface conductivity.[27]

Shielding and discharging effects observed in the ion mode for negative potentials are based on similar processes: secondary electrons resulting from ion impacts on the coverglass would not affect the current characteristics. The presence of a negative potential barrier (Fig. 3) and the lack of anomalous currents confirms secondary emission from the dielectric material as the main effect. Significant secondary emission from the metallic interconnectors in the ion mode is excluded since it would result in increased current collection. Secondary plasma electrons generated by energized primary plasma electrons in the potential barrier region are not important in the global current collection process, since the positive slope of the barrier near the module prevents these electrons from reaching the interconnectors directly.

VI. Conclusions

Interactions between solar array test modules at high bias voltage and the LEO plasma have been shown to be determined by the combined interfaces of conducting and dielectric materials in the plasma environment. The generation of local surface potentials on the dielectric coverglasses and strong electric fields in the interconnect environment turn out to be the driving mechanism for anomalous current collection and arc discharges.

The test results support the hypothesis that the anomalous current increase at high positive voltages above 300 V is caused by secondary electron emission from the coverglass edges. Under the given test conditions, it was not possible to obtain a complete snap-over of the interconnector potential across the full coverglass area. Moreover, the test results provide evidence for the generation of additional ions in front of the surface at certain positive bias voltage levels.

Finally, it is concluded that the relevant surface properties of the test modules require an exposure to the plasma environment for several hours before they stabilize, i.e., before stationary current voltage characteristics are obtained. This equilibrium is again modified if the bias voltage is raised to very high levels, where arc discharges occur.

References

[1]Purvis, C. K., Stevens, N. J., and Berkopec, F. D., "Interaction of Large High-Power Systems with Operational Orbit Charged-Particle Environments," NASA TM-3867, 1977.

[2]Stevens, N. J., Berkopec, F. D., Purvis, C. K., Grier, N., and Staskus, I., "Investigation of High-Voltage Spacecraft System Interactions with Plasma Environments," AIAA Paper 78-672, 1987.

[3]Carruth, M. P., Young, L. E., Purvis, C. K., and Stevens, N. J., "Safe II—Large Systems Space Plasma Evaluation Experiment," AIAA Paper 83-26903, 1983.

[4]Stevens, N. J., "Space Environmental Interactions with Biased Spacecraft Surfaces, Space Systems and their Interactions with Earth's Space Environment," *Progress in Astronautics and Aeronautics: Space Systems and their Interactions with Earth's Space Environment*, Vol. 71, edited by H. B. Garrett and C. P. Pike, AIAA, New York, 1980.

[5]Grier, N. T., "Dilute Plasma Coupling Currents to a High-Voltage Solar Array in Weak Magnetic Fields," AIAA Paper 83-26903, 1983.

[6]McCoy, J. E., Konradi, A., and Garriott, O. K., "Current Leakage for Low-Altitude Satellites," AIAA Paper 79-0387, 1979.

[7]Stillwell, R. P., Kaufman, H. R., and Robinson, R. S., "Experimental Simulation of Space Plasma Interactions with High Voltage Solar Arrays," AIAA Paper 81-0741, 1981.

[8]Ijichi, K., Fujii, H., Gohnai, T., Gotoh, M., Abe, T., Ogata, Y., Obara, H., and Kuriki, K., "High Voltage Solar Array for MPD Propulsion System," AIAA Paper 85-2047, 1985.

[9]Katz, I., Mandell, M. J., Schnuelle, G. W., Parks, D. E., and Steen, P. G., "Plasma Collection by High-Voltage Spacecraft at Low Earth Orbit," *Journal of Spacecraft and Rockets*, Vol. 18, Jan–Feb. 1981, p. 79.

[10]Nonnast, J. H., Chaky, R. C., Armstrong, T. P., Enoch, J., and Wiseman, G. G., "Numerical Simulation of Plasma-Insulator Interac-

tions in Space, Part I: The Self-Consistent Calculation," NASA CP-2182, AFGL TR-81-0270, 1980, pp. 932–945.

[11]Chaky, R. C., Nonnast, J. H., Armstrong, T. P., Enoch, J., and Wiseman, G. G., "Numerical Simulation of Plasma-Insulator Interactions in Space, Part II: Dielectric Effects," NASA CP-2182, AFGL TR-81-0270, 1980.

[12]Stillwell, R. P., Robinson, R. S., and H. R., Kaufman, "Current Collection from the Space Plasma through Defects in Solar Array Insulation," *Journal of Spacecraft and Rockets*, Vol. 22, Nov.–Dec. 1985, pp. 631–641.

[13]Thiemann, H., and Bogus, K., "Anomalous Current Collection and Arcing of Solar Cell Modules in a Simulated High-Density LEO-Plasma," *ESA Journal*, Vol. 10, No. 1, March 1986.

[14]Stevens, N. J., "Interactions between Large Space Power Systems and Low-Earth-Orbit Plasma," NASA CP-2359, 1983.

[15]Cap, F., "Einführung in die Plasmaphysik," Vol. 1, Akademie-Verlag, Berlin, 1970, p. 18.

[16]Laframboise, J. G., "Theory of Spherical and Cylindrical Langmuir Probes in a Collisionless Maxwellian Plasma at Rest," UTIAS Rept. 100, 1966.

[17]McCoy, J. E. and Konradi, A., "Sheath Effects Observed on a 10-Meter High-Voltage Panel in a Simulated Low Earth Orbit Plasma," NASA CP-2071, 1979.

[18]Gabriel, S. B., Garner, C. E., and Kitamura, S., "Experimental Measurements of the Plasma Sheath around Pinhole Defects in a Simulated High-Voltage Solar Array," AIAA Paper 83-0311, 1983.

[19]Eichmeier, J., *Moderne Vakuumelektronik*, Springer Verlag, Berlin, 1981.

[20]Levy, L., Sarrail, D., and Signeir, J. M., "Conductivity and Secondary Emission Properties of Dielectrics as Required by NASCAP," European Space Agency SP-232, Oct. 1985, pp. 43–124.

[21]Leung, M. S., Tueling, M. B., and Schnauss, E. R., "Effects of Secondary Electron Emission on Charging," NASA CP-2182, 163, 1981.

[22]Chaky, R. C., Nonnast, J. H., Armstrong, T. P., Enoch, J., and Wiseman, G. G., "Numerical Simulation of Plasma Insulator Interactions in Space, Part II: Dielectric Effects," NASA CP-2181, 1980, pp. 946–956.

[23]Snyder, D., "Discharges on a Negatively Biased Solar Cell Array in a Charged-Particle Environment," NASA CP-2359, 1983.

[24]Grier, N., "Experimental Results on Plasma Interactions with Large Surfaces at High Voltages," NASA TM-81423, 1980.

[25]Neske, E. and Kist, R., "Impedance Probe, the AEROS-B Electron Density Experiment," *Zeitschrift für Geophysik*, Vol. 40, No. 5, 1974, pp. 593–600.

[26]Spenner, K. and Dumbs, A., "The Retarding Potential Analyser on AEROS-B," *Journal of Geophysical Research*, Vol. 40, 1974, pp. 585–592.

[27]Brandon, T., Kessel, R. L., Enoch, J., and Armstrong, T. P., "Numerical Simulations of Positively Biased Probes and Dielectric-Conductor Peaks in a Plasma," *Journal of Applied Physics*, Vol. 56, 1984, p. 3215.